

Self-Starting Lithium Niobate Soliton Microcombs

CNF Project Number: 1997-11

Principal Investigator(s): Qiang Lin

User(s): Yang He, Rui Luo, Jingwei Ling

Affiliation(s): Department of Electrical and Computer Engineering, University of Rochester

Primary Source(s) of Research Funding: Defense Threat Reduction Agency-Joint Science and Technology Office for Chemical and Biological, Defense (grant No. HDTRA11810047), National Science Foundation under grants No. ECCS-1810169 and ECCS1610674

Contact: qiang.lin@rochester.edu, yhe26@ur.rochester.edu, ruiluo@rochester.edu, jling8@ur.rochester.edu

Primary CNF Tools Used: JEOL 9500, Yes Asher, AJA, DISCO dicing saw

Abstract:

We report soliton generation in a high- Q lithium niobate resonator. The photorefractive effect enables self-starting mode locking and is able to produce stable single solitons on demand that feature reversible switching between soliton states.

Summary of Research:

The recent demonstration of soliton mode locking in microresonators [1] represents a major turning point in the subject of frequency microcombs and many material systems and cavity geometries are being explored for various applications [2]. In this work soliton generation in a high- Q lithium niobate (LN) resonator is observed for the first time. Moreover, on account of the intriguing properties of lithium niobate the soliton mode locked system is able to self-start. Specifically, soliton microcombs must be pumped at a frequency that is red detuned relative to a cavity resonance [2], but this regime is also unstable due to a thermo-optical nonlinearity [3]. As a result special techniques for pumping and triggering solitons have been developed [2]. Here the photorefractive property of LN is shown to allow stable operation and pumping on the red-detuned side of resonance. As a result, self-starting mode locking of soliton microcombs is demonstrated by a simple and reversible pump tuning process.

LN features a strong photorefractive effect, which causes an intensity-dependent decrease of refractive index [4]. Moreover, LN exhibits a negligible thermo-optic coefficient for the ordinary polarized light (around room temperature) [5], leading to a suppressed thermo-optic nonlinearity. The combination of these two effects results in a net decrease of refractive index with increased optical intensity. This behavior is opposite to that induced by thermo-optic and/or optical Kerr nonlinearities in conventional Kerr soliton microresonators [2]. The optical Kerr effect from the soliton shifts the resonance towards the red, while the photorefractive effect significantly shifts the resonance towards the blue. As a result, the soliton formation regime resides directly

within the laser detuning regime that is self-stabilized by the photorefractive effect, thereby enabling self-starting soliton mode locking.

To show this capability, we used a LN microresonator (shown as Figure 1), which has a radius of 100 μm . The group velocity dispersion of the device is engineered to be slightly anomalous. The device was patterned by electron-beam lithography (JEOL 9500).

To produce Kerr combs, a pump power of 33 mW is coupled onto the chip. When the pump frequency is scanned into a cavity resonance from long wavelength, the average intracavity power readily shows clear discrete steps (Figure 2). Figure 3 shows the spectrum measured for the single soliton at the first power step, which exhibits a smooth hyperbolic sech-shaped spectral envelope.

References:

- [1] T. Herr, et al., "Temporal solitons in optical microresonators," *Nature Photon.* 8, 145-152 (2014).
- [2] T. J. Kippenberg, A. L. Gaeta, M. Lipson, and M. L. Gorodetsky, "Dissipative Kerr solitons in optical microresonators," *Science* 361, 567 (2018).
- [3] T. Carmon, L. Yang, K J Vahala, et al., "Dynamical thermal behavior and thermal self-stability of microcavities," *Optics Express* 12, 4742-4750 (2004).
- [4] P. Gunter and J.-P. Huignard, eds., *Photorefractive Materials and Their Applications* 1, 2 (Springer, New York, 2006).
- [5] L. Moretti, M. Lodice, F. G. D. Corte, and I. Rendina, "Temperature dependence of the thermo-optic coefficient of lithium niobate, from 300 to 515 K in the visible and infrared regions," *J. Appl. Phys.* 98, 036101 (2005).

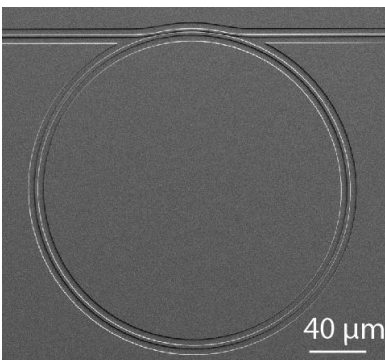


Figure 1: Scanning electron microscope image of a LN microring resonator.

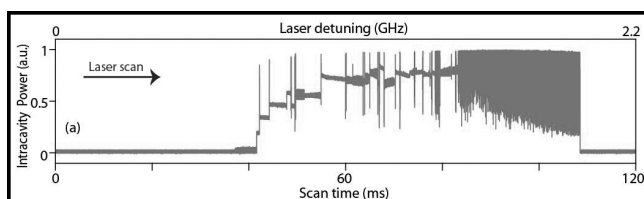


Figure 2: Intracavity power as a function of time when the laser is scanned from red to blue (long to short wavelength).

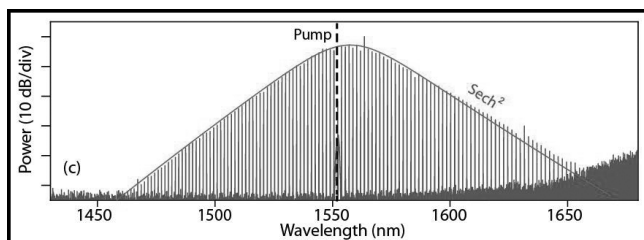


Figure 3: Optical spectrum of the single soliton state.

High-Q Two-Dimensional Lithium Niobate Photonic Crystal Slab Nanoresonators

CNF Project Number: 1997-11

Principal Investigator(s): Qiang Lin

User(s): Mingxiao Li

Affiliation(s): Electrical and Computer Engineering, University of Rochester

Primary Source(s) of Research Funding: National Science Foundation (NSF) (EFMA-1641099, ECCS1810169, and ECCS-1842691); the Defense Threat Reduction Agency-Joint Science and Technology Office for Chemical and Biological Defense (grant No. HDTRA11810047)

Contact: qiang.lin@rochester.edu, mli53@ur.rochester.edu

Primary CNF Tools Used: JEOL 9500, AJA ion mill

Abstract:

We report a 2D LN PhC slab nanoresonators with high optical Q over 3×10^5 . Such a high quality enables us to probe the intriguing anisotropy of nonlinear optical phenomena of LN never reported previously.

Summary of Research:

Photonic crystal (PhC) nanoresonators exhibit exceptional capability of controlling light confinement and light matter interactions in the sub-wavelength scale, which forms a crucial foundation for many applications [1,2]. Among various photonic crystal structures, two-dimensional (2D) photonic crystal slabs exhibit significant advantage in the engineering of the density of photonic states. These excellent characteristics have excited tremendous interest in recent years to develop 2D PhC slab nanoresonators on a variety of material platforms.

Lithium niobate (LN), exhibits outstanding electro-optic, nonlinear optical, acousto-optic, piezoelectric, photorefractive, pyroelectric, and photoconductive properties [5], promising for broad applications. The great application potential has attracted significant attention recently to develop LN photonic devices on chip-scale platforms [3,4,7]. However, realizing high-quality 2D LN PhC structures remains significant challenge [6], which becomes the major obstacle hindering the exploration of optical phenomena in the nanoscopic scale that would potentially result in intriguing device characteristics and novel functionalities inaccessible by conventional means.

In this paper, we demonstrate 2D LN PhC slab nanoresonators with optical Q up to 3.51×10^5 , about three orders of magnitude higher than other 2D LN photonic crystal nanocavities reported to date [6].

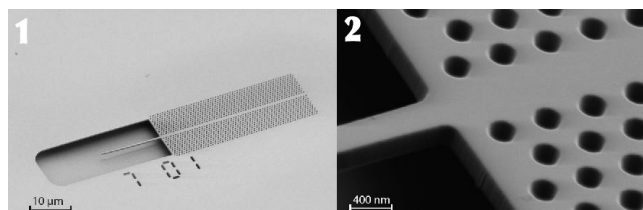


Figure 1: Scanning electron microscopic image of a fabricated 2D LN PhC slab. Figure 2: Zoom-in image of a section of the photonic crystal slab.

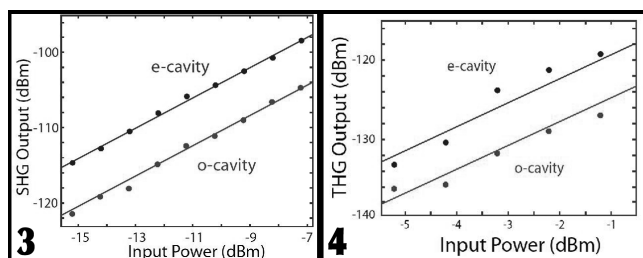


Figure 3: Recorded power of the generated second harmonic wave as a function of that of the fundamental pump wave, where the dots are experimental recorded data for an e-cavity and o-cavity, respectively. The solid lines show quadratic fitting to the experimental data. Figure 4: Recorded power of the generated third harmonic wave as a function of the fundamental pump wave, where the dots are experimental recorded data for an e-cavity and o-cavity, respectively. The solid lines show cubic fitting to the experimental data.

Devices are patterned by JEOL 9500. Such a pure polarization enables us to explore intriguing anisotropy of optical phenomena, by making the line-defect cavity either in parallel with or perpendicular to the optical axis. For convenience, we denote the one perpendicular to the optical axis as an e-cavity since the dominant electric field polarizes along the optical axis, corresponding to the extraordinary polarization. Accordingly, we denote the one in parallel with the optical axis as an o-cavity as the dominant cavity field polarizes along the ordinary polarization. In particular, the high optical Q together with the tiny effective mode volume supports extremely strong nonlinear optical interactions, which results in efficient third harmonic generation combined with cascaded second harmonic generation, for the first time in on-chip LN nanophotonic devices [3,4,7]. The demonstrated high- Q 2D LN PhC nanoresonators offer an excellent device platform for the exploration of extreme nonlinear and quantum optics at single-photon and few-photon level, opening up a great avenue towards future development of energy efficient nonlinear photonic and electro-optic signal processing.

In summary, we have demonstrated 2D LN PhC slab nanoresonators with optical Q up to 3.51×10^5 that is about three orders of magnitude higher than other 2D LN PhC nanoresonators reported to date [6]. The high optical Q together with tight optical mode confinement results in intriguing nonlinear optical interactions. We have observed second-harmonic generation, particularly third harmonic generation that is the first time to be observed in on-chip LN nanophotonic devices [3,4,7].

Moreover, the devices exhibits pure polarization of the cavity modes, which enabled us to probe the intriguing anisotropy of nonlinear optical phenomena, which have never been reported previously.

References:

- [1] E. Kuramochi, K. Nozaki, A. Shinya, K. Takeda, T. Sato, S. Matsuo, H. Taniyama, H. Sumikura, and M. Notomi, "Large-scale integration of wavelength-addressable all-optical memories on a photonic crystal chip," *Nature Photon.* 8, 474 (2014).
- [2] P. Lodahl, S. Mahmoodian, and S. Stobbe, "Interfacing single photons and single quantum dots with photonic nanostructures," *Rev. Mod. Phys.* 87, 347 (2015).
- [3] R. Luo, H. Jiang, H. Liang, Y. Chen, and Q. Lin, "Self-referenced temperature sensing with a lithium niobate microdisk resonator," *Opt. Lett.* 42, 1281 (2017).
- [4] C. Wang, X. Xiong, N. Andrade, V. Venkataraman, X.-F. Ren, G.-C. Guo, and M. Loncar, "Second harmonic generation in nanostructured thin-film lithium niobate waveguides," *Opt. Express* 25, 6963 (2017).
- [5] R. S. Weis and T. K. Gaylord, "Lithium niobate: Summary of physical properties and crystal structure," *Appl. Phys. A* 37, 191-203 (1985).
- [6] R. Geiss, S. Diziain, M. Steinert, F. Schrepel, E.-B. Kley, A. Tunnermann, and T. Pertsch, "Photonic crystals in lithium niobate by combining focused ion beam writing and ion-beam enhanced etching," *Phys. Stat. Sol. A* 211, 2421 (2014).
- [7] H. Liang, et al., "High-quality lithium niobate photonic crystal nanocavities," *Optica.* 4, 1251 (2017).

Fabrication of Anti-Resonant Reflecting Optical Waveguides for On-Chip Raman Spectroscopy

CNF Project Number: 2255-13

Principal Investigator(s): Jin Suntivich^{1,2}

User(s): Chengyu Liu³

Affiliation(s): 1. Materials Science and Engineering Department, 2. Kavli Institute at Cornell for Nanoscale Science, 3. School of Applied and Engineering Physics; Cornell University

Primary Source(s) of Research Funding: Samsung Advanced Institute of Technology (SAIT)

Contact: js2765@cornell.edu, CL986@cornell.edu

Primary CNF Tools Used: AJA sputter deposition, Woollam spectroscopic ellipsometer, ABM contact aligner, SC4500 evaporator, Oxford PECVD

Abstract:

On-chip gas sensing technology has received extensive attention due to its potential applications in environmental and healthcare monitoring. Herein, we utilize hollow-core anti-resonant reflecting optical waveguides (ARROWs) in the near-infrared wavelength for on-chip Raman scattering for various chemical detections. In this work, we fabricate hollow-core ARROWs with Bragg reflectors made by tantalum oxide (Ta_2O_5) and silicon dioxide (SiO_2) film decks and characterize our device performance. The propagation loss is about 19 dB/cm at 780 nm wavelength, which is an advance for the next-generation integrated on-chip Raman sensors.

Summary of Research:

On-chip sensing technology [1,2] has received extensive attention due to its potential applications in environmental and healthcare monitoring. On-chip spectroscopy methods such as on-chip infrared absorption spectroscopy have high sensitivity and selectivity; however, on-chip infrared devices still face challenges from the component complexity and cost. Herein, we use hollow-core anti-resonant reflecting optical waveguides (ARROWs) [3,4] in the near-infrared wavelength for on-chip Raman scattering for gaseous-molecule detections. The geometry of the hollow-core ARROWs confines the guided light in the air mode, where the optical field can efficiently overlap with the detected molecules. To demonstrate the proof of concept, we fabricate hollow-core ARROWs with alternating layers of Ta_2O_5 and SiO_2 , where the fabrication details will be discussed.

We first designed the Bragg reflector by alternating Ta_2O_5 and SiO_2 layers. A period of high index/low index dielectric film decks can provide a desirable reflectance over a certain range. We utilized the transfer matrix method to simulate the film decks with different design parameters. Considering the fabrication difficulty, we limit the $\text{Ta}_2\text{O}_5/\text{SiO}_2$ period number to be three. We got the actual film thicknesses for each layer by Woollam ellipsometer and measured the reflectance of deposited

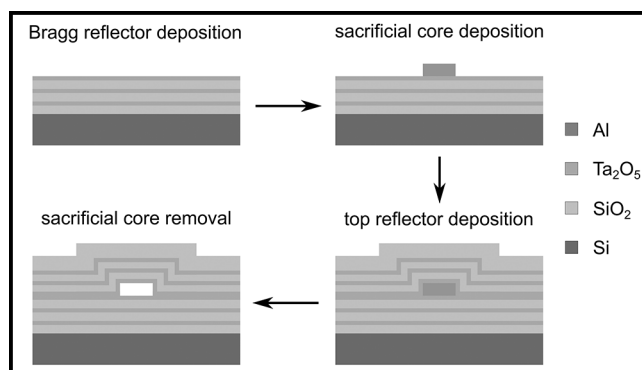


Figure 1: The fabrication process of ARROW waveguides.

film decks with UV/Vis/NIR optical spectrophotometer to verify our design (results not shown). The thicknesses used for each layer were optimized to reach the maximum reflection near 800 nm wavelength.

After that, we developed the fabrication process shown in Figure 1 for the ARROWs. We started with a silicon wafer. First, we deposited a stack of Ta_2O_5 and SiO_2 Bragg layers using sputtering (Ta_2O_5 using reactive sputtering

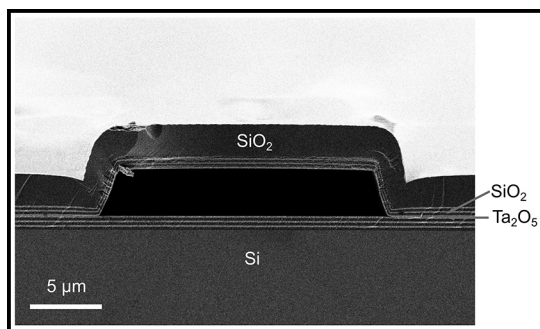


Figure 2: An SEM image of the hollow core structure after aqua regia etching.

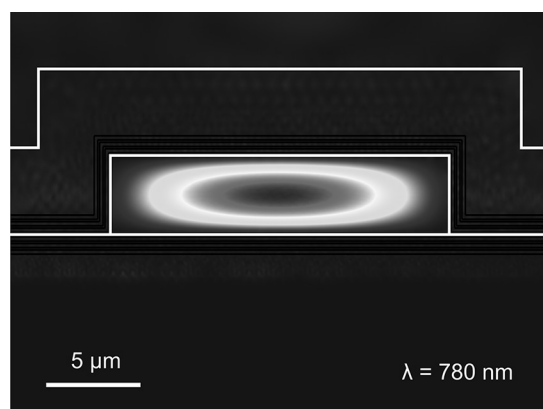


Figure 3: Calculated guiding mode profile of the ARROW waveguide at 780 nm.

and SiO₂ using RF sputtering) based on our calibrated design parameters. Then, we did a contact lithography for waveguide sacrificial core patterning. A 3.5- μm thick aluminum (Al) was evaporated into these patterned channels. Then, we did a lift-off to remove the unwanted Al to form the sacrificial channels. Similarly, a Bragg reflector by Ta₂O₅ and SiO₂ was deposited on top of the Al channels. A 3- μm thick protective oxide cladding was added by PECVD. After a clean facet cleaving, Al sacrificial cores were removed by a two-day heated aqua regia etching in our lab.

Figure 2 shows a representative scanning electron micrograph (SEM) of the fabricated ARROW waveguide after aqua regia etching, which exemplifies a hollow core feature of our device.

We design the ARROWs by calculating the mode profile using the geometry estimated from SEM (Figure 2). The modal behavior was calculated from a commercial mode solver assuming that an air core inside. Figure 3 indicates that our fabricated ARROW waveguide supports a quasi-TE mode inside the air core, which provides the complete mode overlap between the pump mode and Stokes mode. In order to characterize this device's performance, we measured the propagation loss using a top-view camera method around 780 nm wavelength in air. Using the background-corrected signals, we fit the loss data to a regression model. The propagation loss of our device is about 19 dB/cm. To characterize the feasibility of the ARROW as a waveguide-based evanescent Raman sensor for gaseous molecule detection, we are incorporating a flow cell, where external gases can be applied to the device.

In conclusion, we propose a hollow-core ARROW structure by Ta₂O₅ and SiO₂ for on-chip Raman sensing especially for gas detection. We have fabricated the proposed ARROW waveguides with a clear hollow core and the device has been characterized. Future work will focus on the device application for gaseous molecule sensing.

References:

- [1] Dhakal, A., Subramanian, A. Z., Wuytens, P., Peyskens, F., Le Thomas, N., and Baets, R. (2014). Evanescent excitation and collection of spontaneous Raman spectra using silicon nitride nanophotonic waveguides. *Optics letters*, 39(13), 4025-4028.
- [2] Evans, C. C., Liu, C., and Suntivich, J. (2016). TiO₂ Nanophotonic sensors for efficient integrated evanescent Raman spectroscopy. *ACS Photonics*, 3(9), 1662-1669.
- [3] Yin, D., Schmidt, H., Barber, J. P., and Hawkins, A. R. (2004). Integrated ARROW waveguides with hollow cores. *Optics Express*, 12(12), 2710-2715.
- [4] Schmidt, H., Yin, D., Deamer, D. W., Barber, J. P., and Hawkins, A. R. (2004, October). Integrated ARROW waveguides for gas/liquid sensing. In *Nanoengineering: Fabrication, properties, optics, and devices* (Vol. 5515, pp. 67-81). International Society for Optics and Photonics.

High Quality Factor PECVD Si_3N_4 Ring Resonators Compatible with CMOS Process

CNF Project Number: 2364-15

Principal Investigator(s): Michal Lipson

User(s): Xingchen Ji, Samantha Roberts

*Affiliation(s): Department of Electrical Engineering, Columbia University, New York, NY 10027;
School of Electrical and Computer Engineering, Cornell University, Ithaca, NY 14853*

Primary Source(s) of Research Funding: Defense Advanced Research Projects Agency

Contact: ML3745@columbia.edu, xj53@cornell.edu, spr2127@columbia.edu

Primary CNF Tools Used: PECVD, e-beam lithography, Oxford 100 etcher, AJA sputter deposition

Abstract:

We demonstrate high-confinement Si_3N_4 resonators with intrinsic quality factors more than one million using standard PECVD process. We show that by addressing scattering, the loss at 1.6 μm can be as low as 0.4 dB/cm.

Summary of Research:

High quality factor silicon nitride (Si_3N_4) ring resonators are critical for a variety of applications such as low threshold frequency combs [1-3], high precision sensing [4] and optical communications [5]. To date, high quality factor Si_3N_4 ring resonators have been demonstrated almost solely using Si_3N_4 films with high stress, deposited using low-pressure chemical vapor deposition (LPCVD), a high temperature process. Both the high stress of the films and the high temperature process make the fabrication of these devices in a standard foundry challenging.

Plasma-enhanced chemical vapor deposition (PECVD) is a standard, low temperature, commercial process for depositing low stress films. Indeed, achieving low waveguide losses in PECVD Si_3N_4 has been challenging. There have been efforts to reduce losses in PECVD Si_3N_4 films by substituting conventional precursors to deuterated precursors [6], which requires specialized tools and a series of complicated tests. Using standard PECVD, compatible with CMOS processes, the lowest propagation loss reported to date without a high temperature long furnace anneal are 1.6 dB/cm at 1.55 μm and 2.5 dB/cm at 1.6 μm [7,8].

Here we demonstrate Si_3N_4 ring resonators with intrinsic quality factors of more than one million using a standard PECVD process. We show that processes addressing scattering losses such as optimized etch process, chemical-mechanical planarization (CMP) and multipass lithography can lead to quality factors above 700,000.

When combined with rapid thermal anneal (RTA) which reduces film absorption loss, quality factors can be more than one million. In contrast to furnace anneal, rapid thermal anneal has been successfully applied in the microelectronics industry. This has particular relevance for CMOS technology, specifically process steps such as implant annealing, oxidation, source and drain contact junctions [9].

We fabricated our devices on a thermally oxidized 4-inch silicon wafer. Si_3N_4 is deposited using PECVD at 350°C in a single step. CMP, a standard CMOS process, is applied to Si_3N_4 top surface in order to reduce scattering from top surface. The roughness before and after CMP is shown in Figure 1 and Figure 2. The roughness is reduced from 1.36 nm to 0.20 nm. In order to reduce the roughness from the sidewalls, we use a SiO_2 hard mask deposited using PECVD after CMP and use a dry etching process with a higher oxygen flow. This etching process has been shown to reduce substantially the polymerization process during etching and decrease losses [3]. We pattern our devices with electron beam lithography using ma-N 2403 resist and use multipass to further reduce sidewall roughness from lithography. We clad the devices with 2 μm of SiO_2 using PECVD. After cladding, we applied RTA at 800°C for 5 mins to reduce absorption loss.

We have achieved an intrinsic quality factor of more than one million using the optimized process. The fabricated devices have radius of 115 μm , height of

730 nm and width of 1500 nm coupled to a waveguide of the same dimensions. These dimensions ensure high confinement. The mode simulation and fabricated devices are shown in Figure 1. In order to test the devices, we launch a tunable laser source, transmitted through a fiber polarization controller, into the inverse nanotaper of our device using a lensed fiber and collect the output of the ring resonator through another inverse nanotaper with a collimating lens. We then monitor the output on a photodetector. Figure 3 shows the measured normalized transmission spectrum before RTA. The measured intrinsic quality factor around $1.6 \mu\text{m}$ is 724,000, corresponding to a propagation loss of 0.42 dB/cm. Figure 4 shows the measured normalized transmission spectrum after RTA. The measured intrinsic quality factor around $1.6 \mu\text{m}$ is 1.08 million, corresponding to a propagation loss of 0.28 dB/cm. Therefore, simply by addressing the surface roughness, we are able to achieve propagation loss as low as 0.42 dB/cm. After RTA, we achieve even lower loss of 0.28 dB/cm.

Utilizing CMOS compatible processes including etch optimization, CMP, multipass lithography and RTA, we are able to fabricate low loss waveguides and ring resonators. We have achieved high quality factor more than one million using a standard PECVD process. This work provides a platform for achieving low loss, crack-free Si_3N_4 films, which could greatly benefit applications such as 3D photonic integration, telecommunications and nonlinear processing.

References:

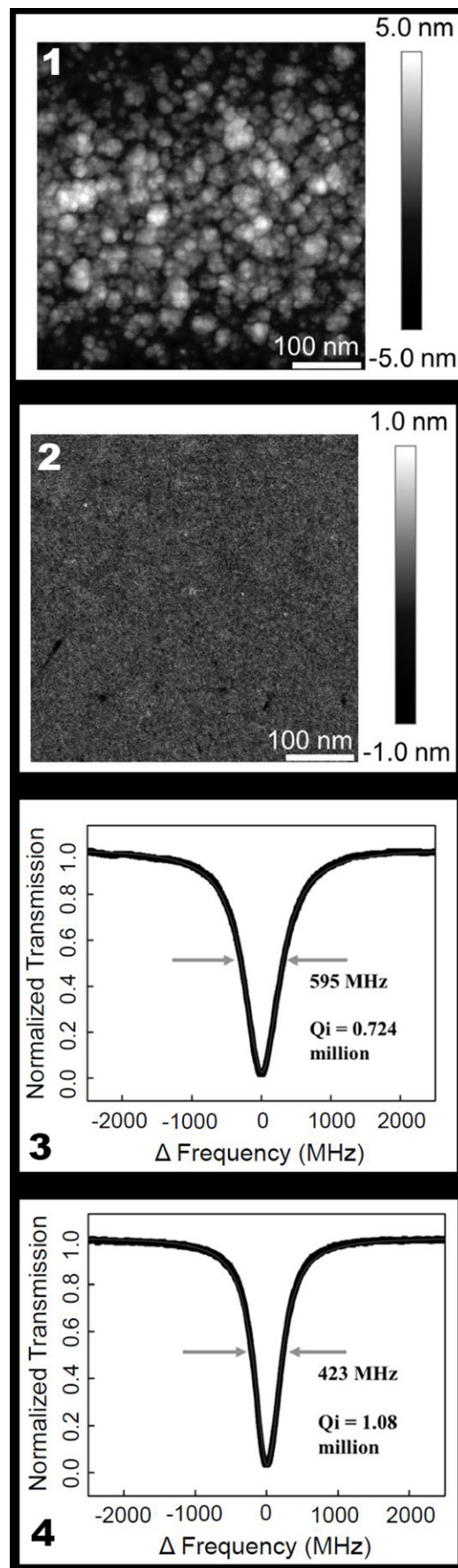
- [1] B. Stern, X. Ji, Y. Okawachi, A. L. Gaeta, and M. Lipson, *Nature* 562(7727), 401-405 (2018).
- [2] Y. Xuan, et al. *Optica* 3, 1171-1180 (2016).
- [3] X. Ji, et al. *Optica* 4(6), 619 (2017).
- [4] T. Kippenberg, A. L. Gaeta, M. Lipson, and M. L. Gorodetsky, *Science* 361 (6402), (2018).
- [5] P. Marin-Palomo, et al. *Nature* 546(7657), 274-279 (2017).
- [6] J. Chiles, et al. *Optics Letters* 43(7), 1527 (2018).
- [7] E. A. Douglas, et al. *Optical Materials Express* 6(9), 2892 (2016).
- [8] L. Wang, W. Xie, D. V. Thourhout, H. Yu, and S. Wang, *Optics Express* 26, 9645-9654.
- [9] M. J. Hart and A. G. R. Evans, *Semiconductor Science and Technology* 3(5), 421-436 (1988).
- [10] P. Rabiei, W. H. Steier, C. Zhang, and L. R. Dalton, *J. Lightwave Technol.* 20(11), 1968-1975 (2002).

Figure 1: AFM measurement of the top surface of Si_3N_4 before CMP. Roughness of 1.36 nm.

Figure 2: AFM measurement of the top surface of Si_3N_4 after CMP. Roughness of 0.20 nm.

Figure 3: Normalized transmission spectra of the same ring resonator before rapid thermal anneal (RTA). Resonance with 595 MHz linewidth corresponding to an intrinsic Q of 0.72 million.

Figure 4: Normalized transmission spectra of the same ring resonator after rapid thermal anneal (RTA). Resonance with 423 MHz linewidth corresponding to an intrinsic Q of 1.08 million.



III-N UV Photonic Devices

CNF Project Number: 2387-15

Principal Investigator(s): Debdeep Jena

User(s): Shyam Bharadwaj, Kevin Lee, Ryan Page, Jimy Encomendero

Affiliation(s): Electrical and Computer Engineering, Materials Science Engineering; Cornell University

Primary Source(s) of Research Funding: National Science Foundation

Contact: djena@cornell.edu, sb2347@cornell.edu, kl833@cornell.edu, rlp238@cornell.edu, jje64@cornell.edu

Primary CNF Tools Used: ABM contact aligner, electron-beam evaporators, Plasma-Therm PT770

Abstract:

Our research goal is to improve and fabricate deep ultraviolet (DUV) and visible photonic devices such as light-emitting diodes (LEDs) and laser diodes (LDs). We grow the semiconductor thin films by molecular beam epitaxy (MBE). The III-nitride material system is ideal for such devices due to its wide range of direct bandgaps. For deep UV devices, AlN, GaN and AlGaIn are the typical materials. P-type transport is a major challenge in these materials; as such, we are focusing on improving this property through the use of InGaIn contact layers and polarization-doped AlGaIn cladding regions. The structure of the active region is also an important determinant of the external quantum efficiency (EQE) of the LEDs, so we are studying different active region thicknesses and compositions.

Summary of Research:

We grow UV LED structures by plasma-assisted MBE (PA-MBE). These LEDs are grown on metal organic chemical vapor deposition (MOCVD)-grown AlN on sapphire template substrates. One study we performed involved a comparison of AlGaIn active region DUV LEDs to ultra-thin GaN active region ones. Ultra-thin GaN theoretically has a more favorable valence band alignment for light extraction, though AlGaIn active regions can be grown thicker (resulting in a larger active volume — a larger region in which radiative recombination can occur) while still emitting at the same wavelength. The structures that were grown are shown in Figure 1.

After growing the LED structures, they were processed in the CNF using contact photolithography. Positive tone photoresist was spun onto samples for the device isolation step. After developing, individual devices were defined through ICP-RIE etching in the PT770 tool. The electron-beam evaporators were used to deposit metal contacts for probing.

After the LEDs were fabricated, the electrical and optical characteristics were measured through current-voltage (IV) and electroluminescence (EL) measurements. The results of these measurements are shown in Figure 2 (IV) and Figure 3 (EL).

It can be seen that that the electrical performance of the devices are fairly similar between the two structures, with current densities reaching ~ 500 A/cm² at 10V. The

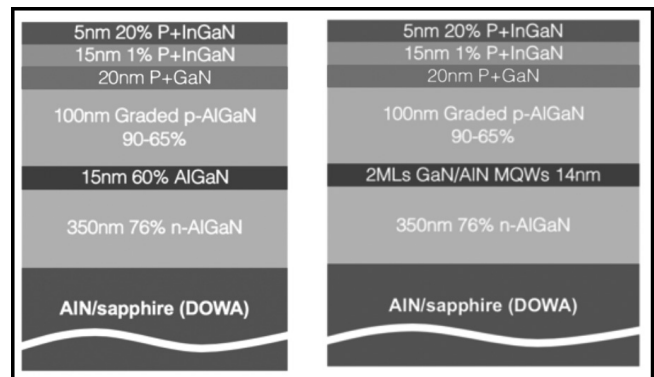


Figure 1: Schematic structures of the UV LEDs grown in this study. On the left is the AlGaIn active region LED, and on the right is the ultra-thin GaN active region LED. The AlGaIn LED has one single quantum well, while the ultra thin GaN LED has 4 quantum wells separated by 2 nm AlN barriers.

biggest difference in device performance can be seen in the EL results: the measured EL intensity for the device with an AlGaIn active region is roughly 10x greater than the EL intensity from the device with GaN active region at the same current levels. This can be partly attributed to the difference in active volume: The AlGaIn device active area is roughly 7x greater than the GaN device active area. More work is being performed to quantify the difference in emission properties (such as the angle- and polarization-resolved emission patterns) of the two active regions.

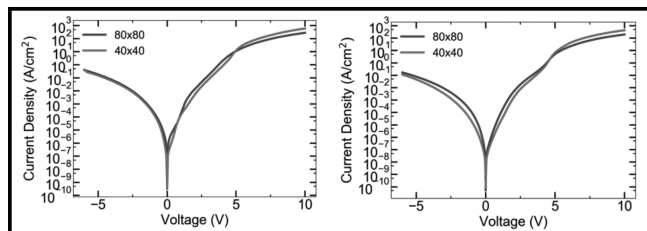


Figure 2: Log scale current-voltage characteristics of the two LEDs. The IV for the AlGaN active region LED is shown on the left, while the IV for GaN active region LED is on the right. Two different device areas were measured for each (80×80 square μm , and 40×40 square μm).

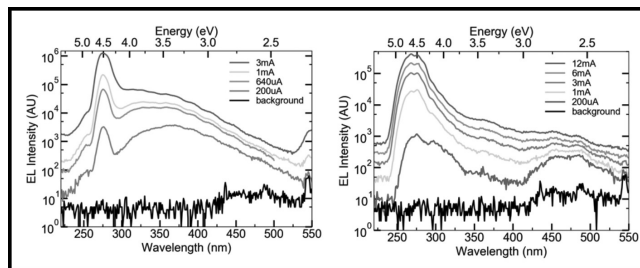


Figure 3: Log scale electroluminescence data for the two LEDs (AlGaN active region device on left, GaN active region device on the right). Both devices have emission peaks around 275 nm, though the AlGaN active region device has a larger broad peak around 375 nm (likely defect related). The AlGaN active region device has around 10x emission intensity as the GaN device for the same current levels.

Development of Single and Double Layer Anti-Reflective Coatings for Astronomical Instruments

CNF Project Number: 2458-16

Principal Investigator(s): Gordon Stacey¹

User(s): Bugao Zou², Nicholas Cothard², Mahiro Abe³

Affiliation(s): 1. Department of Astronomy, 2. Department of Applied and Engineering Physics, 3. Department of Physics; Cornell University

Primary Source(s) of Research Funding: NASA Grant NNX16AC72G

Contact: stacey@cornell.edu, bz332@cornell.edu, nc467@cornell.edu, ma797@cornell.edu

Primary CNF Tools Used: ABM contact aligner, Oxford plasma-enhanced CVD, Anatech resist strip, Oxford 82 etcher, Hamatech-Steag wafer processors, manual resist spinners, resist hot strip bath, Heidelberg mask writer - DWL 2000, Plasma-Therm deep silicon etcher, Zygo optical profilometer, Zeiss Supra/Ultra SEM

Abstract:

We have been developing Fabry-Perot interferometers using silicon-based metal mesh filters for the far infrared and sub-millimeter astronomical instruments. The filters comprise gold meshes on one side and metamaterial anti-reflection coatings on the other side to both achieve wide bandwidth transmission and mitigate Fresnel reflection by the un-metalized substrate surface. In the past year we had a paper presented at SPIE Advances in Optical and Mechanical Technologies for Telescopes and Instrumentation III that demonstrates the performance of metal mesh reflectors and anti-reflection coated silicon surfaces by simulation and establishes standard procedures to fabricate these two parts. We are currently polishing the recipe of anti-reflection coatings by fabricating samples on high-resistivity silicon wafers. We will test the optical efficiency of samples fabricated at CNF using a Fourier transform spectrometer.

Summary of Research:

The purpose of the project is to develop Fabry-Perot interferometers for use in the far infrared and sub-millimeter astronomical instruments. They are comprised of metal mesh reflectors and metamaterial anti-reflection coatings. The former part provides high reflectance over the frequency range of interest and controls the resolving power of interferometers while the latter part help mitigate strong Fresnel reflections of silicon and widen the bandwidth.

Our main job at CNF is the development of the fabrication methods of these two parts. We had some preliminary result about the fabrication of anti-reflection coatings published in Applied Optics a few years ago [1]. Last summer we had a paper presented at SPIE Advances in Optical and Mechanical Technologies for Telescopes and Instrumentation III [2] that summarizes the fabrication procedures for metal meshes and anti-reflection coatings and we continued to refine the recipe in order to improve the performance of samples.

Figure 1 shows two microscope images (taken by CNF's Olympus MX-50 Microscope) of metal mesh filters. We fabricate metal mesh filters using standard evaporation and lift-off lithography techniques. Negative lift-off

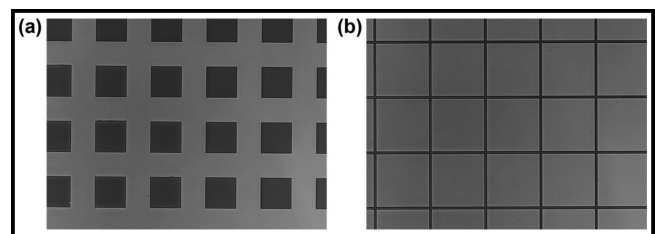


Figure 1: Microscope images of inductive (a) and capacitive (b) metal meshes fabricated by depositing 10 nm of gold on silicon.

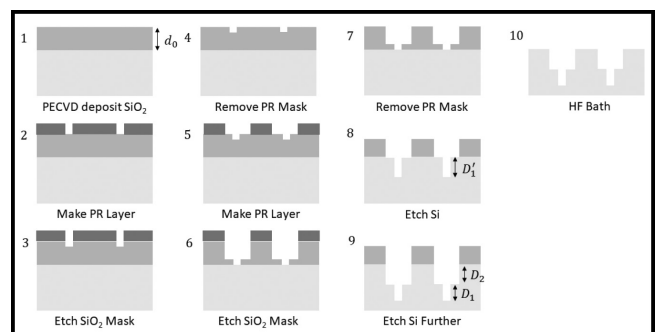


Figure 2: Process flow for fabricating a double-layer ARC on a silicon wafer. Grey represents the oxide. Dark grey represents the photoresist. Light grey represents the silicon wafer.

photoresist (AZ nLOF 2020) is exposed with the mesh pattern using an ABM contact aligner and then developed. The patterned resist is descummed using an Anatech resist strip. After that, 500 nm of gold are evaporated onto the patterned wafer using a CHA evaporator. Then the wafer is placed in a bath of Microposit 1165 remover and left for 24 hours to clean up the photoresist. Using contact lithography, feature sizes of 1 μm can be achieved.

Figure 2 shows our current recipe for double-layer anti-reflection coatings. We start with depositing the silicon dioxide using an Oxford plasma-enhanced chemical vapor deposition (PECVD) tool. Then two photomasks are correspondingly patterned with oxide etch process in between to define the double-layer structure of anti-reflection coatings. The oxide etch process is achieved by a reactive ion etch tool Oxford 82 and those masks are removed using an Anatech resist strip. The lower layer is then etched using a Plasma-Therm deep silicon etcher. Besides, we add an external thermal oxidation step followed by a buffered oxide etch of hydrofluoric acid and an oxygen stripping step after each silicon etch to remove the passivation layer generated during silicon etch

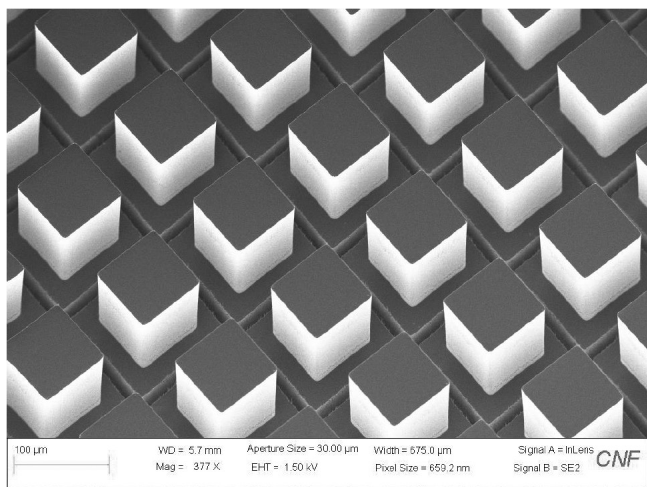


Figure 3: SEM image taken using CNF's Zeiss Ultra SEM showing successful fabrication of our two-layer metamaterial silicon anti-reflection coatings. (See cover.)

processes, which may form fence-like structure at the boundary of two silicon layers. Figure 3 shows an SEM image (taken by CNF's Zeiss Ultra SEM) of a successful result of this fabrication procedure.

The Fabry-Perot interferometers we have been developing will be used in the CCAT-prime telescope located at 5600 meters elevation on Cerro Chajnantor in the Atacama Desert in Chile [3]. One of the science goals of the CCAT-prime telescope is to study the Epoch of Reionization, a time around one billion years after the Big Bang when the first galaxies were assembling. The broad bandwidth of the silicon substrate Fabry-Perot interferometers can efficiently cover the far-IR frequencies required for an intensity mapping of the [CII] fine structure line to probe this era of the universe, and will provide information on the first star forming galaxies.

In the past year we have made great steps towards achieving our goals at CNF. We have demonstrated our ability to fabricate double-layer ARCs for different wavelengths and metal meshes with different feature sizes. We have used many of the fabrication and metrology tools at CNF. Our next steps are to better characterize our etched geometries and improve our metamaterial ARCs. We will be using Fourier transform spectrometers to measure our samples optical performance and using the results to iterate on our fabrication design.

References:

- [1] P.A. Gallardo, B.J. Koopman, N.F. Cothard, S.M.M. Bruno, G. Cortes-Medellin, G. Marchetti, K.H. Miller, B. Mockler, M.D. Niemack, G. Stacey, and E.J. Wollack, "Deep reactive ion etched anti-reflection coatings for sub-millimeter silicon optics," *Appl. Opt.* 56, 2796-2803 (2017).
- [2] N.F. Cothard, M. Abe, T. Nikola, G.J. Stacey, G. Cortes-Medellin, P.A. Gallardo, B.J. Koopman, M.D. Niemack, S.C. Parshley, E.M. Vavagiakis, and K. Vetter, "Optimizing the efficiency of Fabry-Perot interferometers with silicon-substrate mirrors," Presented at SPIE Advances in Optical and Mechanical Technologies for Telescopes and Instrumentation III (2018).
- [3] <http://www.ccatobservatory.org/>

Fabricating All-Glass, 1 cm Diameter Metalens Working at Visible Wavelength

CNF Project Number: 2471-16

Principal Investigator(s): Professor Federico Capasso

User(s): Joon-Suh Park

Affiliation(s): John A. Paulson School of Engineering and Applied Sciences, Harvard University

Primary Source(s) of Research Funding: Defense Advanced Research Projects Agency

Contact: capasso@seas.harvard.edu, parkj@g.harvard.edu

Website: <https://www.seas.harvard.edu/capasso>

Primary CNF Tools Used: Heidelberg DWL2000, Hamatech mask chrome etch 1, ASML 300C DUV stepper, Gamma automatic coat-develop tool, CVC sputter, CHA Mark 50 e-beam evaporator, Trion Minilock III ICP etcher, Oxford 81, Oxford 82, Oxford 100, P10 profilometer, Zeiss Ultra SEM

Abstract:

Single-material, centimeter-scale metalens working in the visible wavelength is demonstrated in mass-manufacturing style. Using DUV stepper lithography, we show wafer-scale fabrication of a flat optical elements capable of diffraction-limited focusing at visible wavelength.

Summary of Research:

With the market growth of virtual reality (VR), augmented reality (AR), or mixed reality (MR) devices, aerial drone cameras, and on-board cameras for orbital satellites, the importance of payload for optical devices is evermore increasing. However, as such applications need large-aperture optics to meet its physical demands such as the size of the human eye's pupil, or to obtain better imaging in low-light conditions by increasing the amount of collected light. For conventional refractive optics, aperture size and the weight were in trade-off relations: The larger the aperture, the heavier the lens become at an undesirable rate. In addition, due to the nature of refractive optics where the optics relied on the refractive index of the lens material and its curvature at the material boundary, they were subject to spherical aberration (Figure 1). Such aberration was dealt with using expensive methods such as creating aspheric surfaces, cascading multiple lenses, choosing high-refractive materials, or using size-limiting variables such as using aplanatic point.

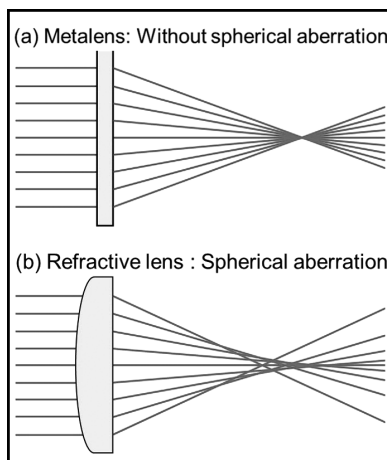


Figure 1: Effect of spherical aberration to focusing profiles. (a) Metalens, without spherical aberration. (b) Refractive lens, with spherical aberration.

In our previous reports [1,2], we have shown that metasurfaces, a new class of optics that rely on sub-wavelength structures capable of locally controlling the output phase, amplitude, and polarization, can pave way to an alternative solution for refractive optics. By placing sub-wavelength structures on a planar surface, one can design an optical component that resembles the functionality of a refractive optics counterpart. Many prior works presented in the field of metasurfaces used deposition of high-refractive index dielectrics, such as TiO_2 , SiN , GaN , amorphous silicon, and such, to achieve such functionalities. In this research, we instead use fused silica (SiO_2) wafer, a low-refractive index material, and demonstrate a metasurface lens (metalens) capable of focusing and imaging as a lens in the visible wavelength.

To fabricate such lens, we choose DUV (248 nm, KrF) stepper lithography so that we can create features smaller than the incident wavelength. At CNF, we use Heidelberg DWL 2000 mask writer to create a reticle of the metalens. After writing the mask design by exposing the photoresist with UV laser scanner on a chrome-coated quartz reticle blank, we develop the photoresist using Hamatech mask chrome etch 1. After optical inspection of the developed pattern on the reticle, we wet-etch the chrome layer with the patterned photoresist as etch mask. The reticle substrate is chosen to fit the ASML 300C DUV stepper.

The substrate on which the metalens is fabricated is chosen to be a 4-inch fused silica wafer, as most of the tools in CNF are set to work with 4-inch wafers. On top, we deposit a thin-layer of chrome, with either CVC sputter (decommissioned) or CHA Mark 50 e-beam evaporator. After coating AR3 ARC layer and DUV resist using GAMMA automatic coat-develop tool (GAMMA), we expose the substrate with the metalens pattern written on the reticle, using ASML 300C DUV stepper. The exposed wafer is then put through post-exposure bake, develop, rinse, and dry process with the GAMMA tool. After ensuring the focus-dose conditions with the DUV stepper, we perform descum and ARC layer etch using Oxford 81 or 82 etcher. Then, we transfer the pattern to the chrome layer by plasma etching, using Trion Minilock III ICP-etcher. When the metalens pattern is transferred to the chrome layer, we remove the DUV resist and the ARC layer using Oxford 81 or 82 etcher, using oxygen plasma. The SiO_2 wafer is then plasma etched with the patterned chrome as etch mask, using Oxford 100 etcher until we reach the target etch depth. We inspect the fabrication results with P10 profilometer and Zeiss Ultra SEM. The fabrication of the metalens is completed when we then remove the chrome layer, leaving only SiO_2 pattern (Figure 2). From our measurements, we observe that the fabricated metalens show diffraction-limited focusing in the visible wavelength (Figure 3), and high-quality imaging properties.

The results of this research are being prepared for publication.

References:

- [1] A. She, S. Zhang, S. Shian, D.R. Clarke, and F. Capasso, "Large area metalenses: design, characterization, and mass manufacturing," *Opt. Express* 26, 1573-1585 (2018).
- [2] M. Khorasaninejad, W.T. Chen, R.C. Devlin, J. Oh, A.Y. Zhu, and F. Capasso, "Metalenses at visible wavelengths: Diffraction-limited focusing and subwavelength resolution imaging," *Science* 352, 1190 (2016).

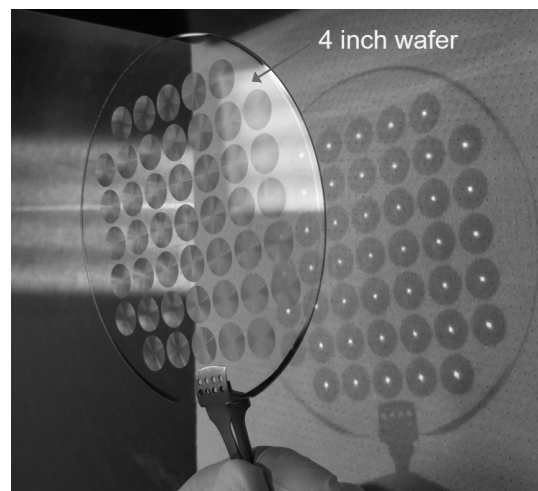


Figure 2: Photograph of fabricated metalens with diameter of 1 cm, on a 4-inch fused silica wafer.

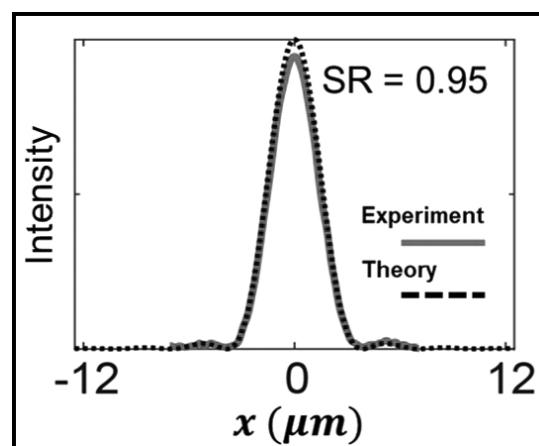


Figure 3: Focusing profile of the metalens.

Metasurface-Based Infrared Optical Devices

CNF Project Number: 2472-16

Principal Investigator(s): Gennady Shvets

User(s): Melissa Bosch, Minwoo Jung, Maxim Shcherbakov

Affiliation(s): School of Applied and Engineering Physics, Department of Physics; Cornell University

Primary Source(s) of Research Funding: Office of Naval Research (ONR) and National Science Foundation (NSF)

Contact: gs656@cornell.edu, mb2583@cornell.edu, mj397@cornell.edu, mrs356@cornell.edu

Website: <http://shvets.aep.cornell.edu>

Primary CNF Tools Used: JEOL 9500, CVC SC4500 evaporator, Zeiss Supra SEM

Abstract:

Planar metamaterials, or metasurfaces, provide strong and resonant light modulations both in near- and far-fields. We engineer several metasurface structures for near-to mid-infrared photonic applications. A plasmonic metasurface, for example, can be integrated with graphene to greatly enhance the absorption of incident radiation into graphene through ultrahigh field enhancement at its resonance. On the other hand, we also exploit low-loss dielectric metasurfaces with thermally tunable resonances to demonstrate tunable polarization control. These metasurface-based approaches are scalable and space-efficient, thereby promising versatile platforms for ultrathin optical devices.

Summary of Research:

High-Gain and High-Speed Mid-Infrared Graphene Photodetector with Plasmonic Metasurfaces.

Graphene, owing to its gapless and semi-metallic electronic dispersion, is a broadband photo-diode, and graphene photodetectors can be in principle operated at ultrahigh speeds up to hundreds of gigahertz thanks to its linear Dirac electrons traveling at a relatively high Fermi velocity [1]. High-gain operation, however, is not guaranteed in graphene itself due to its monolayer nature and weak absorption. Strong field enhancement via resonant metasurfaces can increase the absorption into graphene by an order of magnitude without sacrificing high-speed capability [2]. We aim for even more efficient high-gain configuration, by using the metasurface structures themselves as the electrodes—source and drain—of the photodetector. In this way, the gain is enhanced not only due to the plasmonic resonances, but also by reducing the distance that the photo-generated carriers travel to get to the electrodes.

Furthermore, as seen in Figure 1, the source and the drain are interdigitated, thus increasing the photo-absorption area by a factor of the number of metasurface unit cells. The device is fabricated in a total of five e-beam lithography steps: (1) alignment marks, (2) graphene patterning, (3) source deposition, (4) drain deposition, and (5) contact pads deposition. The source and the drain are deposited in separate steps for introducing different materials (Ti and Pd) for the adhesion layer between graphene and gold. Two different contact metals dope graphene at slightly different Fermi levels, enabling

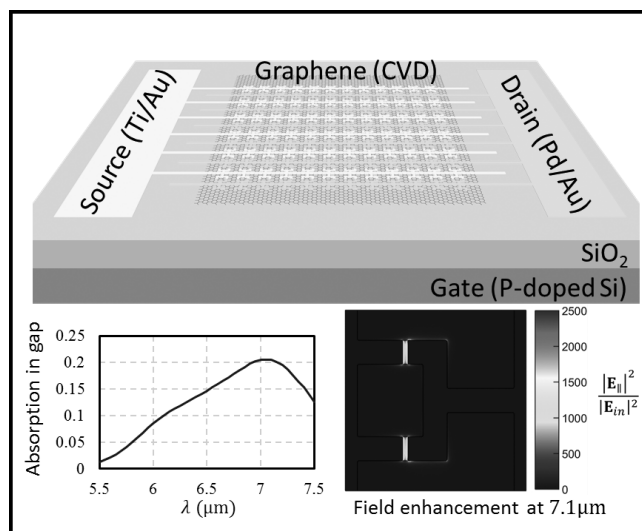


Figure 1: Top, Schematic of graphene photodetector integrated with a plasmonic metasurface. Bottom Left, Absorption of mid-infrared radiation into graphene in the gap region between the source and drain. Bottom Right, Field enhancement at the plasmonic resonance.

photo-voltaic mode operation at zero source-drain bias voltage.

Figure 2 shows an SEM image zoomed on a gap between the source and the drain. The fabricated device is currently under electrical and optical characterization. Our simulation predicts a photocurrent of ~ 0.1 A/W at the resonance.

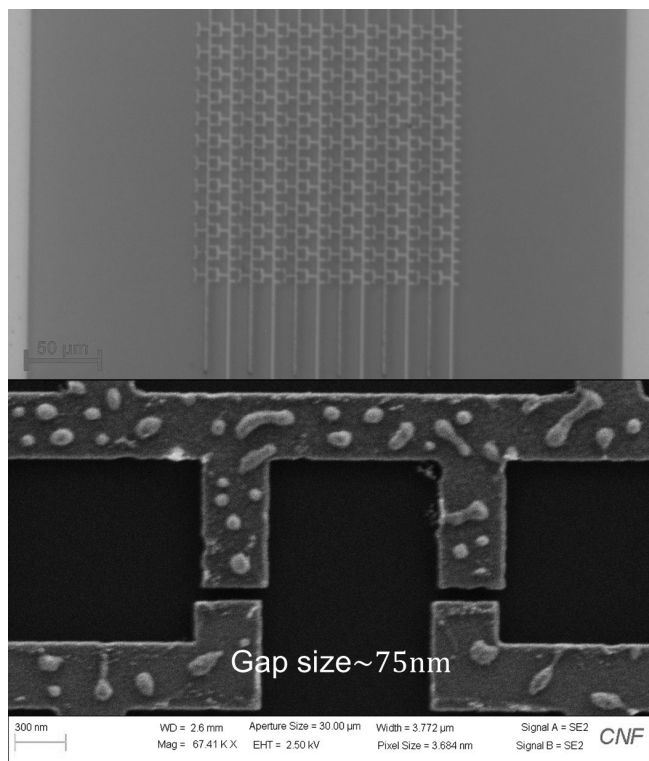


Figure 2: Top, Fabricated device imaged under optical microscope. Bottom, SEM image zoomed on a gap between the source and the drain.

Polarization States Synthesizer Based on a Thermo-Optic Dielectric Metasurface. The dynamic control of light polarization is ubiquitous to free-space and integrated photonics applications. Low-loss dielectric metasurfaces have recently emerged as an attractive platform for efficient polarization synthesizers, however most implementations exhibit static functionalities. Germanium (Ge), one of the most promising materials for nanophotonics [3] due to its infrared transparency and high refractive index, also has one of the largest thermo-optic coefficients in the mid-infrared range [4].

In our work, we exploit the thermo-optic properties of germanium to demonstrate a resonant dielectric metasurface that acts as a thermally-actuated polarization state generator. This is accomplished through the design of a germanium-based anisotropic resonant metasurface (ARM) which supports a spectrally-sharp (high- Q) resonance that can be excited by one of the principal linear polarizations of incident light. Enabled by the high thermo-optic coefficient of germanium, the central frequency of the high- Q mode can be adjusted by almost its bandwidth within a 100°C window. Due to the anisotropic nature of the mode, light that is initially linearly polarized becomes elliptically polarized upon transmission through the ARM, with a polarization state that can be widely tuned by heating the sample. For device fabrication, we use the following procedure: a standard two-layer PMMA spin-coat, baking, and e-beam

exposure at 1000 $\mu\text{C}/\text{cm}^2$ (JEOL 9500); development in MIBK:IPA 1:3 for 90s; e-beam evaporation of 300 nm of Ge (CVC SC4500), and liftoff in room-temperature sonicated acetone for 60s.

Figure 3 presents an SEM image of the fabricated metasurface and its temperature-dependent transmittance spectra. An example of the experimental thermal polarization tuning is shown in Figure 4; by varying both temperature and the polarization angle of incident light, we find the full polarization tuning range of the device covers near 40% of the upper Poincare hemisphere surface.

References:

- [1] Photodetectors based on graphene, other 2D materials and hybrid systems. F. Koppens, T. Mueller, P. Avouris, A. Ferrari, M. Vitiello and M. Polini; Nature Nanotechnology 9, 780-793 (2014).
- [2] High-Responsivity Mid-Infrared Graphene Detectors with Antenna-Enhanced Photocurrent Generation and Collection. Y. Yao, R. Shankar, P. Rauter, Y. Song, J. Kong, M. Loncar, and F. Capasso; Nano Letters 14(7), 3749-3754 (2014).
- [3] Mid-infrared photonics in silicon and germanium. Soref, Richard; Nature photonics 4.8 (2010): 495.
- [4] Temperature-dependent refractive index of silicon and germanium. Frey, B.J., D.B. Leviton, and T.J. Madison; Optomechanical technologies for Astronomy. Vol. 6273. International Society for Optics and Photonics, 2006.

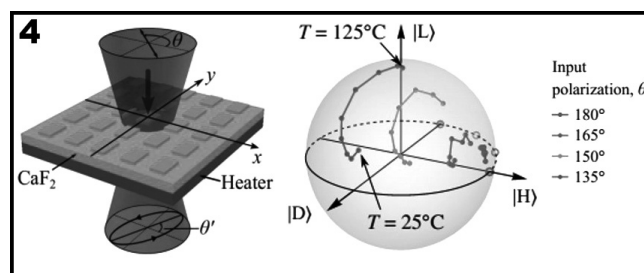
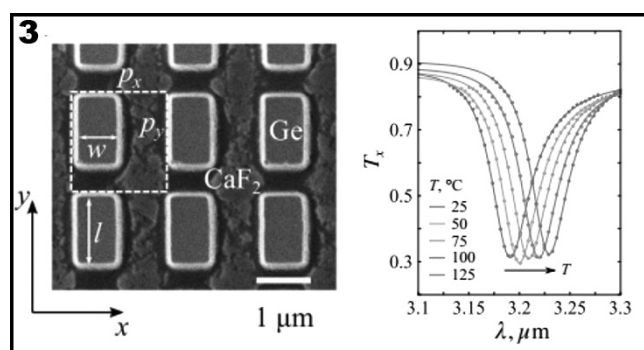


Figure 3, top: Left, An SEM image of the fabricated metasurface. Right, Experimental temperature-dependent mid-IR transmittance spectra of the metasurface, with Q -factor near 70.

Figure 4, bottom: Left, Schematic depicting the temperature-tunable polarization conversion of light transmitted through the ARM. Right, A Poincare sphere depicting the maps of experimental polarization modulation by the metasurface at a wavelength of 3.21 μm , corresponding to the maximum Poincare sphere coverage. Individual curves describe the transformation of the transmitted polarization state with increasing metasurface temperature for different incident polarizations.

Exploratory Etching and Electrodeposition Project

CNF Project Number: 2527-17

Principal Investigator(s): Dr. David Crouse

User(s): Golsa Mirbagheri

Affiliation(s): Electrical and Computer Engineering Department, Clarkson University

Primary Source(s) of Research Funding: CFM, Clarkson University

Contact: dcrouse@clarkson.edu, mirbagg@clarkson.edu

Primary CNF Tools Used: Oxford 82, Oxford 100, ASML, Gamma, PECVD, Cobra

Abstract:

This project is a continuing project. We will be finishing the fabrication of the hyperbolic metamaterial structure and designing a 2nd generation of the filter that uses more of a photonics crystal resonant material within a Bragg stack. Both the hyperbolic metamaterial structure and the 2nd generation devices have compelling properties. Both show very little dispersion — meaning that their performance is not affected by the angle of incidence to the optical signal.

Project Description:

During the last year, we have further designed the hyperbolic metamaterial device and have performed much more optimization and have taken into account practical design considerations. We are now fabricating the structure at the Cornell NanoScale Science and Technology Center (CNF). We have developed a fabrication plan and are now implementing the plan, with masks designed and fabrication processes in development. Based on what we have learned, we are now investigating a 2nd generation device that does not use metal wires, but uses resonant cavities in the three middle layers of the Bragg stack.

The resulting structure will have far less polarization dependence, will absorb less radiation, will be far easier to fabricate and manufacture, and will have a larger tuning range that allows for it to be used within pixelated wavelength filters for hyperspectral imaging applications.

We have been performing preliminary testing on the resonant cavities and have a preliminary design for operation in the midwavelength infrared range of 3-5 μm . The Bragg stack will use silicon and silicon dioxide, and potentially silicon nitride — all CMOS compatible devices — as well as having all structure features with sizes amenable to optical lithography.

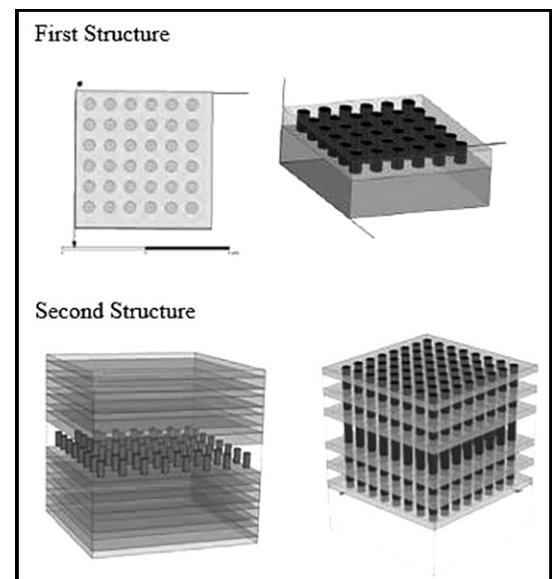


Figure 1: First Structure: The 1.5 μm SiO_2 film was deposited, patterned and etched. The holes were 0.5 μm , electroplated with Cu. Second Structure: Alternative layers of SiO_2 and Si are deposited, patterned and etched (all through the layers), then holes electroplated with Cu.

Metamaterial Spectrometer: A Low SWaP, Robust, High Performance Hyperspectral Sensor for Land and Atmospheric Remote Sensing

CNF Project Number: 2661-18

Principal Investigator and User(s): Lori Lepak

Affiliation(s): Phoebus Optoelectronics LLC

Primary Source(s) of Research Funding: NASA

Contact: llepak@phoebusopto.com

Website URL (Optional): www.phoebusopto.com

Primary CNF Tools Used: DWL2000 photomask writer, ASML stepper, JEOL 9500 e-beam lithography, AJA sputter, Oxford PECVD, SC4500 evaporators, Oxford Cobra etcher, Oxford 81 etcher, Trion etcher, CMP, SEM, Woolam ellipsometer, DISCO dicing saw

Abstract:

Since 2003, Phoebus Optoelectronics has enabled custom R&D solutions in the fields of Plasmonics, Metamaterials, Antennas, and Sensors. We work closely with our customers throughout device development, from prototype realization to small volume manufacturing. Our R&D portfolio spans the spectral ranges of visible light, infrared, terahertz, and microwave radiation, for applications in high resolution infrared imaging systems, wavelength and polarization filtering, tunable optical components, beam forming and steering, solar cells and renewable energy devices, and chemical and biological toxin sensors. Our agile team makes extensive use of the resources at the CNF for our nano/micro fabrication and testing, to provide cost efficiency and rapid turnaround. In the present report, we discuss the ongoing development of a metamaterial-based hyperspectral imaging filter.

Summary of Research:

Phoebus uses the resources of the CNF to fabricate plasmonic chips patterned with a metamaterial surface to enable Extraordinary Optical Transmission (EOT), a phenomenon unique to metastructures in which light is transmitted through apertures much smaller than the incident wavelength, at anomalously large intensities relative to the predictions of conventional aperture theory. EOT was first observed by T.W. Ebbesen in 1998 [1]. Since its founding in 2003, Phoebus has successfully harnessed EOT by incorporating metasurfaces into devices used to perform light filtering [2-3], photon sorting [4-5], polarimetric detection [6], high speed optical detection [7], and most recently, in our SPR plasmonic sensor chips [8].

Examples of metastructured optical devices previously fabricated by Phoebus at CNF are shown in Figures 1-3. In our first-generation IR polarimeter (Figure 1), which is currently commercially available, each pixel has four arrays of wires oriented at 0°, 45°, 90°, and 135° to each other. Each array is capable of acting as a graded index lens, to focus and collimate transmitted light. At the same time, the phase delay produced by the four arrays together allow the pixel as a whole to behave as a polarizer to control the phase of the light. A higher magnification image of a typical array (Figure 2) illustrates the high aspect ratios and smooth sidewalls which are essential

for the high-quality performance of our metasurface structures. A second generation of this design, which was fabricated by electron beam lithography and tailored to operate at a shorter wavelength, is shown in Figure 3.

In our current project, we are developing a hyperspectral imaging system, shown schematically in Figure 4. Our technology (Figure 4b) uses a metasurface to precisely target very narrow spectral bands of interest, enabling a significant reduction in the size and number of optical components relative to current state-of-the-art imaging systems (Figure 4a), which in turn will enable integration of our high-performance sensor onto weight-sensitive platforms (ie. satellites) far more readily than existing systems. The goal of our initial application is to detect and image trace gases in the Earth's atmosphere in the midwave infrared (MWIR) region, with a reduction to adjacent channel latency of less than 10 ms. In planned future research, the overall metasurface technology can be easily adapted to other spectral ranges, from the visible to the microwave, by substituting appropriate materials (most of which can be deposited in the CNF), and scaling feature sizes of the metastructures in proportion to the desired wavelength of imaging. Thus, our versatile Metamaterial Spectrometer technology is expected to be applicable to a much broader range of imaging and sensing applications.

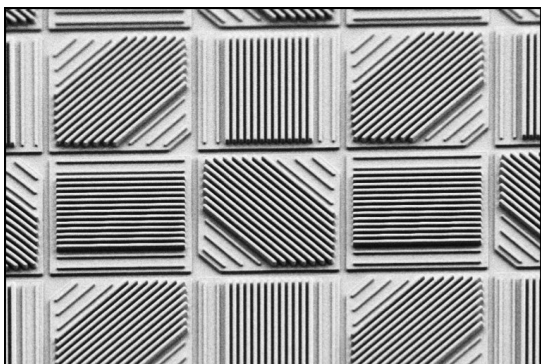


Figure 1: SEM image of metasurface-based IR polarimeter, currently commercially available from Phoebus, and initially developed at CNF using the ASML DUV stepper.

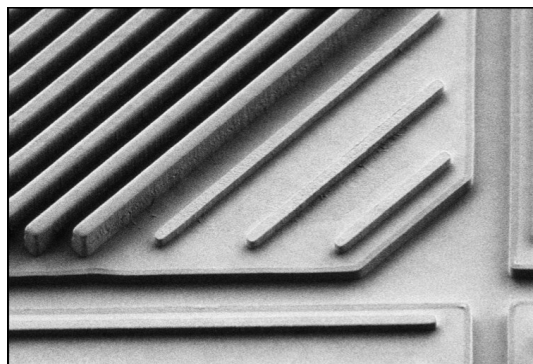


Figure 2: A single sub-pixel at higher magnification. These high aspect ratio features with smooth sidewalls were fabricated at CNF using the ASML DUV stepper and dry etch tools.

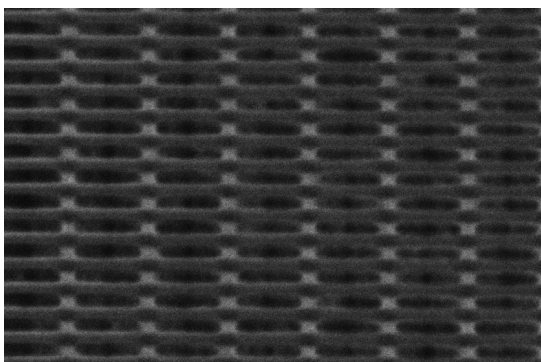


Figure 3: SEM image of another focusing polarimeter device developed by Phoebus at CNF, fabricated using the JEOL 9500 e-beam lithography system.

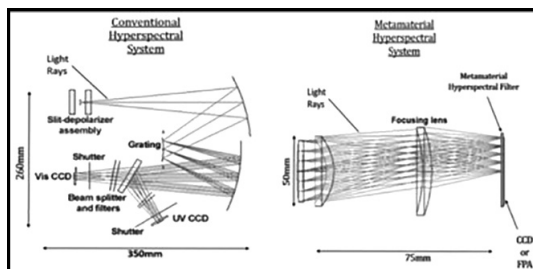


Figure 4: Phoebus's Metamaterial Spectrometer (MS) technology eliminates much of the size and weight of current hyperspectral spectrometer technologies.

References:

- [1] Ebbesen, T.W., et al., "Extraordinary optical transmission through sub-wavelength hole arrays." *Nature*, 391(6668): p. 667-669 (1998).
- [2] Crouse, D. "Numerical modeling and electromagnetic resonant modes in complex grating structures and optoelectronic device applications." *Electron Devices, IEEE Transactions on* 52.11: 2365-2373 (2005).
- [3] Crouse, D., and Keshavareddy, P. "Polarization independent enhanced optical transmission in one-dimensional gratings and device applications." *Optics Express* 15.4: 1415-1427 (2007).
- [4] Lansy, E., Crouse, D., et al. "Light localization, photon sorting, and enhanced absorption in subwavelength cavity arrays." *Optics Express* 20.22: 24226-24236 (2012).
- [5] Jung, Y.U.; Bendoyim, I.; Golovin, A.B.; and Crouse, D.T. "Dual-band photon sorting plasmonic MIM metamaterial sensor." *Proc. SPIE 9070, Infrared Technology and Applications XL, 90702X*; doi:10.1117/12.2050620 (June 24, 2014).
- [6] Crouse, D., and Keshavareddy, P. "A method for designing electromagnetic resonance enhanced silicon-on-insulator metal-semiconductor-metal photodetectors." *Journal of Optics A: Pure and Applied Optics* 8.2: 175 (2006).
- [7] Mandel, I.; Gollub, J.; Bendoyim, I.; Crouse, D. Theory and Design of A Novel Integrated Polarimetric Sensor Utilizing a Light Sorting Metamaterial Grating. *Sensors Journal, IEEE: Vol. PP, 99* (2012).

